Title

Stick–slip friction of gecko-mimetic flaps on smooth and rough surfaces

Journal

Journal of The Royal Society Interface, 12(104)

ISSN

1742-5689

Authors

Das, Saurabh
Cadirov, Nicholas
Chary, Sathya
et al.

Publication Date

2015-03-01

DOI

10.1098/rsif.2014.1346

INTERFACE

rsif.royalsocietypublishing.org

Research

Cite this article: Das S, Cadirov N, Chary S, Kaufman Y, Hogan J, Turner KL, Israelachvili JN. 2015 Stick–slip friction of gecko-mimetic flaps on smooth and rough surfaces. *J. R. Soc. Interface* **12**: 20141346.
http://dx.doi.org/10.1098/rsif.2014.1346

Received: 9 December 2014
Accepted: 16 December 2014

Subject Areas:
biomaterials, biomimetics, synthetic biology

Keywords:
stick–slip friction, gecko-mimetic, rough surface friction

Authors for correspondence:
Kimberly L. Turner
e-mail: turner@engineering.ucsb.edu
Jacob N. Israelachvili
e-mail: jacob@engineering.ucsb.edu

†These authors contributed equally to this study.

Electronic supplementary material is available at http://dx.doi.org/10.1098/rsif.2014.1346 or via http://rsif.royalsocietypublishing.org.

THE ROYAL SOCIETY PUBLISHING

Stick–slip friction of gecko-mimetic flaps on smooth and rough surfaces

Saurabh Das[1,†], Nicholas Cadirov[1,†], Sathya Chary[2], Yair Kaufman[1], Jack Hogan[1], Kimberly L. Turner[2] and Jacob N. Israelachvili[1]

[1]Department of Chemical Engineering, and [2]Department of Mechanical Engineering, University of California, Santa Barbara, CA 93106, USA

The discovery and understanding of gecko 'frictional-adhesion' adhering and climbing mechanism has allowed researchers to mimic and create gecko-inspired adhesives. A few experimental and theoretical approaches have been taken to understand the effect of surface roughness on synthetic adhesive performance, and the implications of stick–slip friction during shearing. This work extends previous studies by using a modified surface forces apparatus to quantitatively measure and model frictional forces between arrays of polydimethylsiloxane gecko footpad-mimetic tilted microflaps against smooth and rough glass surfaces. Constant attachments and detachments occur between the surfaces during shearing, as described by an *avalanche* model. These detachments ultimately result in failure of the adhesion interface and have been characterized in this study. Stick–slip friction disappears with increasing velocity when the flaps are sheared against a smooth silica surface; however, stick–slip was always present at all velocities and loads tested when shearing the flaps against rough glass surfaces. These results demonstrate the significance of pre-load, shearing velocity, shearing distances, commensurability and shearing direction of gecko-mimetic adhesives and provide us a simple model for analysing and/or designing such systems.

1. Introduction

Reversible adhesives, which exhibit high adhesion and minimal effort to detach, are vital to systems that need to stick and detach repeatedly with high speeds for fast movement. Smart and reversible adhesives are in growing demand for use in responsive robotics that can climb on walls and ceilings in precarious environments. The motivation for this specialized type of adhesive comes from the long observed ability of geckos to effortlessly run and climb on trees, rocks, walls and ceilings and maintain attachment while stationary and in motion. The gecko's ability to adhere and climb so flawlessly stems from the hierarchical structure of their toe pads and the mechanism they use to actuate and disengage this very high adhesion. The hierarchical system of the toe pads can form and adhere to micro- and nanoasperities on rough surfaces and create a clean contact, and the reliance of van der Waals forces can allow geckos to adhere to hydrophobic and hydrophilic surfaces as long as the polarizability of the surface is not low (e.g. Teflon) [1–3].

The mechanisms for attachment and high adhesive forces of gecko spatula and setae have been measured and modelled by Johnson–Kendall–Roberts (JKR)-type theories [4,5], whereas the ease of detachment from surfaces requires a peel-off theory [6–8]. The effects of end-shape and size of microfibres on adhesion have been investigated experimentally [9,10] and theoretically [11]. It has been found that the frictional forces (parallel to the surface) also contribute to the adhesive force (perpendicular to the surface), giving rise to the model of frictional adhesion. According to this model, the adhesion of a gecko footpad [12] or its mimic to a substrate depends on the applied shear force [4,6] and explains the very low detachment forces observed in climbing geckos. Anisotropic fibrillar synthetic adhesives mimicking the gecko footpad functionality have been previously fabricated [5,13–24] and were used to study adhesion and frictional properties on silica surfaces. The mechanism of operation of these structures involved application of a

Table 1. Comparison of roughness of borosilicate glass discs used to shear against the gecko-mimetic adhesive flaps. Roughness values were measured using an atomic force microscope (see the electronic supplementary material).

disc	avg. height of asperities (μm)	avg. distance between asperities (μm)	avg. slope of asperity edges	RMS roughness (nm)
smooth	<0.01	n.a.	n.a.	11 ± 10
rough	0.33 ± 0.06	6.7 ± 3.5	0.80 ± 0.45	133 ± 20
very rough	0.52 ± 0.09	1.5 ± 1.5	1.2 ± 0.9	308 ± 56

small pre-load (several millinewtons) followed by shearing the structures against the surface of interest for several micrometres to allow the real surface area of contact to be maximized and hence attain a good grip. However, the stick–slip between the structured surface and the substrate was not taken into consideration during the shearing process in any of the previous work on gecko-mimetic structures. Stick–slip sliding of surfaces is an undesirable property which can cause catastrophic failure if slip occurs while a robotic device is moving on an inclined surface or inverted ceiling. When a constant force (gravity) is acting on the surfaces, there is no restoring force to 'catch' and reattach the failed adhesion contact. Hence, determining the conditions (sliding velocities, pre-loads, sliding distance of the microstructures during movement of the robot, etc.) for avoiding stick–slip motion during the shearing of structured or patterned surfaces on a substrate is essential.

A common form of friction, stick–slip friction, occurs when the static friction force is higher than the kinetic friction force and is found in everyday phenomena such as squeaking doors or the sound produced from a bow sliding across a violin string. Stick–slip sliding occurs over a certain range of driving velocities when the friction force versus velocity shows a negative slope which also depends on the compliance of the surfaces (electronic supplementary material, figure S1) [25,26]. Stick–slip friction can arise by three different mechanisms during frictional sliding: (i) a rough surface mechanism [27] (topography), (ii) distance-dependent mechanism, and (iii) a phase transition mechanism [28]. The first model describes when a rapid slip occurs as one surface goes over the top of an asperity on the opposing surface after 'sticking' for the period owing to interlocks prior to the slip. The distance-dependent model describes how a characteristic distance and time scale are observed as two surfaces increase adhesion strength after coming into contact, which may occur for smooth or rough surfaces. During shearing, the surfaces creep the characteristic distance before sliding occurs. These systems are related to the Deborah number, *De*, which relates the intrinsic relaxation times of the materials to the time scales of movement and measurement in the system [25,29]. The time scales can easily be converted to a characteristic relaxation velocity and sliding velocity in the system. Lastly, the phase transition model is typically only present in lubricated systems or thin films confined between two surfaces which do not pertain to the presented system.

In this study, the friction properties of tilted biomimetic gecko flaps were investigated by measuring and characterizing the friction force as a function of the applied loads and shearing velocities using a surface forces apparatus (SFA) in order to determine the optimum shearing conditions against smooth and rough surfaces. Here, we also propose an *avalanche mechanism* of stick–slip friction. We attribute the stick–slip behaviour in our system to be a combination of surface topography effects as well as characteristic length and time scales related to the material properties of polydimethylsiloxane (PDMS) and intermolecular forces between PDMS and SiO_2.

2. Results

The effects of normal loads ($F_\perp$) and driving velocities (v) on the stick–slip frictional properties of the synthetic tilted PDMS flaps against silica surfaces of different roughness (table 1) were tested in a modified SFA (SurForce, LLC; figure 1). Here, we characterize the surfaces with different roughness based on the height of the surface features (asperities), the spacing between them, the slope of the features and RMS roughness as shown in table 1.

The fluctuations in the lateral force (or friction force, $F_{||}$) were measured in the SFA, and the changes in the friction properties of the flaps shearing against the silica surface were monitored as v was increased at a given compressive force in the normal direction (pre-load, $F_\perp = L$). A close look at the measured friction forces as a function of time indicates that $F_{||}$ can be resolved into three different components: (i) f_{st}, the stiction spike, (ii) f_s, the static friction force, and (iii) f_k, the kinetic friction force (figure 2).

The stiction spike (f_{st}) is the static friction force that must be overcome before any sliding begins between two stationary surfaces and could be higher or lower than the rest of the friction forces measured during shearing. The kinetic friction force (f_k) and the static friction force (f_s) are the minimal and the maximum magnitude of the measured lateral stresses, respectively, when the surfaces are in relative motion during shearing. The kinetic friction force and static friction force are equal during smooth sliding ($f_s = f_k$) [30]. When referring to stick–slip friction, the static force is the maxima of the friction trace (the 'stick'), and the kinetic friction force is the minima where interfacial sliding occurs (the 'slip'). This distinction between kinetic friction in smooth and stick–slip sliding is important to note, because the measured value of f_k in stick–slip is not necessarily the 'true' value of f_k experienced between the surfaces [31]. It should be noted that the friction force (static and kinetic) increases in magnitude (up to 4 mN) while sliding against the direction of the tilt of the flaps (figure 2*b*). This is due to the small aberrations in the thickness of the PDMS base over which the flaps sit and is an artefact of the fabrication process. However, the friction forces do not change significantly (less than 2 mN) while shearing along the tilt direction owing to the strong adhesion of the flaps to the silica surface and hence the variation in the friction force owing to minor misalignments is minimal.

2.1. Effect of load on friction force at a constant driving velocity ($v = 20$ μm s^{-1})

The tilted PDMS microflaps exhibited smooth sliding ($\Delta f = f_s - f_k = 0$) against a smooth silica disc for $F_\perp \leq 20$ mN and

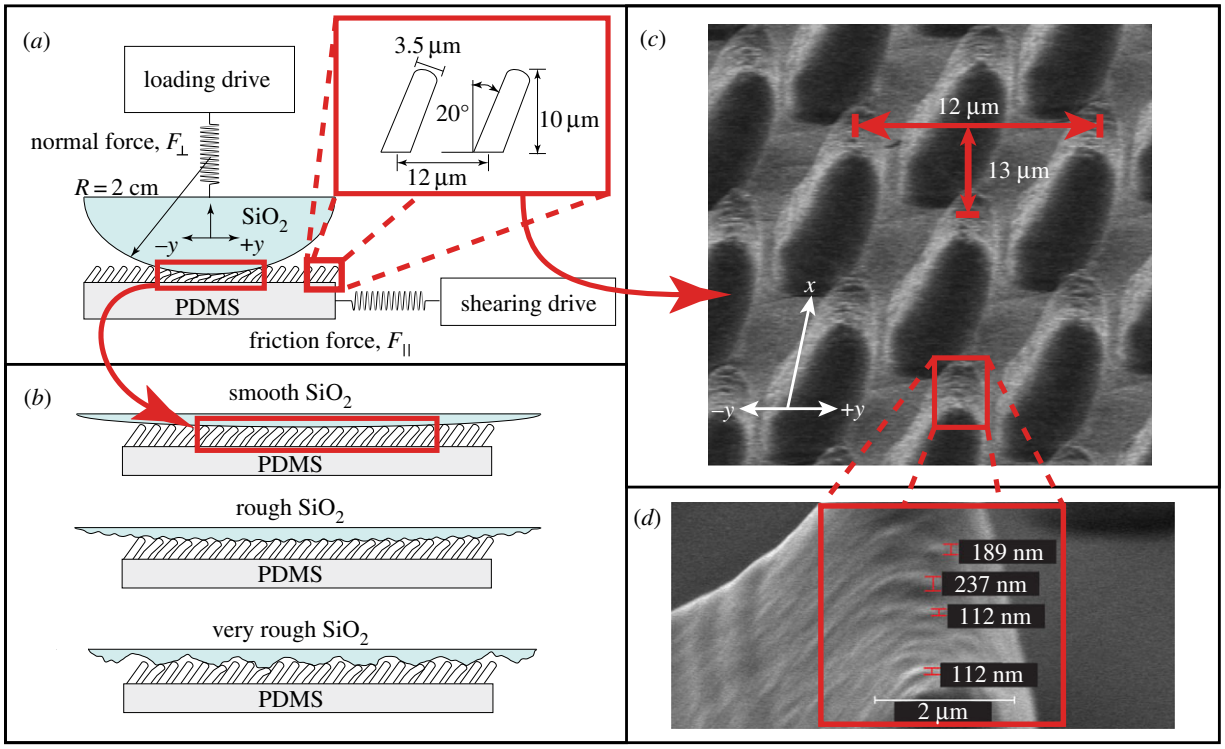

Figure 1. (*a*) Schematic of experimental set-up in the SFA. Two opposing surfaces are sheared against each other: the bottom being the tilted PDMS gecko flaps and the top being the smooth or rough glass disc. (*b*) Schematic of the fitting of PDMS flaps into the different rough disc asperities. There is an interlocking mechanism owing to spacing of the roughness on the glass disc that occurs with the rough (middle) disc. (*c*) Scanning electron microscopy image of the biomimetic flaps depicting the in-plane distribution of the fibrillar structures showing the distance between the flaps along the *x*- and *y*-directions. (*d*) A zoom in on the tip of one pillar depicting submicrometre scale roughness (red bars) on its surface (scale bar in white, 2 µm). (Online version in colour.)

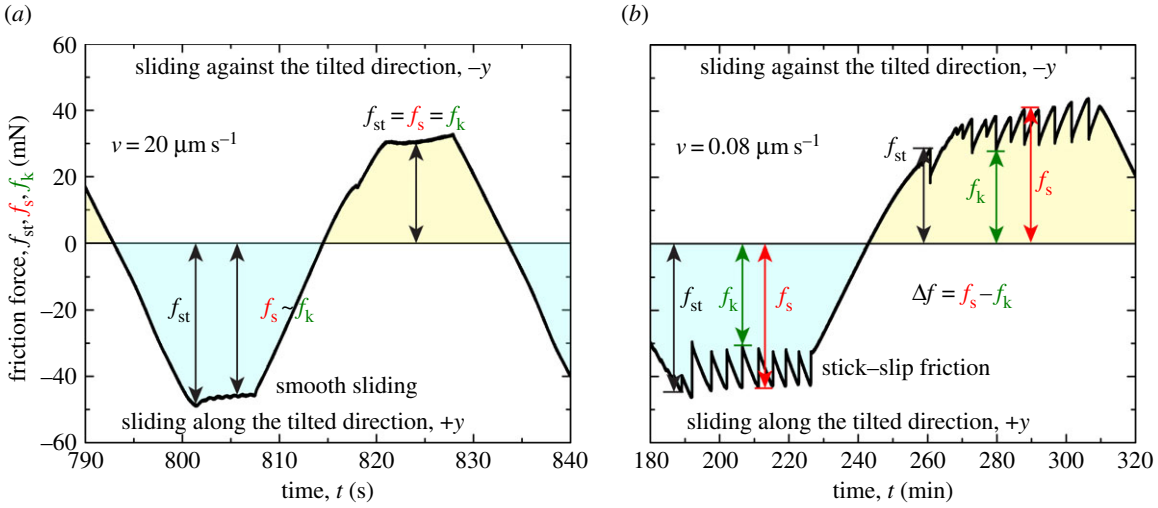

Figure 2. Friction traces of the smooth glass discs with a pre-load *L* approximately 10 mN against gecko-mimetic tilted flaps, where friction forces ($F_{||} = f_{st}, f_s, f_k$) were measured as a function of time. Note that negative forces are not negative in magnitude, but result from the direction of shear during measurement. Smooth sliding (*a*) is observed at velocities greater than 20 µm s^{-1} compared with stick–slip friction which is present at lower drive velocities less than 20 µm s^{-1} (*b*) for the given pre-load. (Online version in colour.)

$v > 20$ µm s^{-1} (figure 3*a*). Stick–slip friction is always observed for the shearing of the flaps against the rough and the very rough silica surfaces for all loads (figure 3*b*,*c*). The friction forces ($F_{||}$) are proportional to the normal loads ($F_\perp$) indicating that Amontons' law is followed [32] in the system under consideration (figure 3*a*,*c*). The coefficient of friction, μ (slope of $F_{||}$ versus $F_\perp$), is higher for sliding of the flaps against the rough (static friction coefficient along $+y$-direction, $\mu_{+y} = 3.4 \pm 0.2$; static friction coefficient $-y$-direction, $\mu_{-y} = 3.5 \pm 0.2$) and the very rough ($\mu_{+y} = 3.1 \pm 0.9$; $\mu_{-y} = 2.5 \pm 0.1$) silica surfaces compared with the smooth surface ($\mu_{+y} = 1.7 \pm 0.7$; $\mu_{-y} = 1.9 \pm 0.9$). The magnitude of stick–slip friction increased as the load increased when shearing the flaps against the rough and the very rough surfaces. Interestingly, the flaps demonstrated similar (within 35% of the highest difference) magnitudes of $F_{||}$ for a given $F_\perp$ on the smooth and the very rough silica surface which is significantly smaller than the $F_{||}$ measured on the rough surface. However, when comparing the magnitude of stick–slip friction, Δf (triangle in lower plots in figure 3), the very rough surface exhibits high values of stick–slip compared with the smooth surface where no stick–slip is observed at any loads ($F_\perp \leq 20$ mN) at $v = 20$ µm s^{-1}.

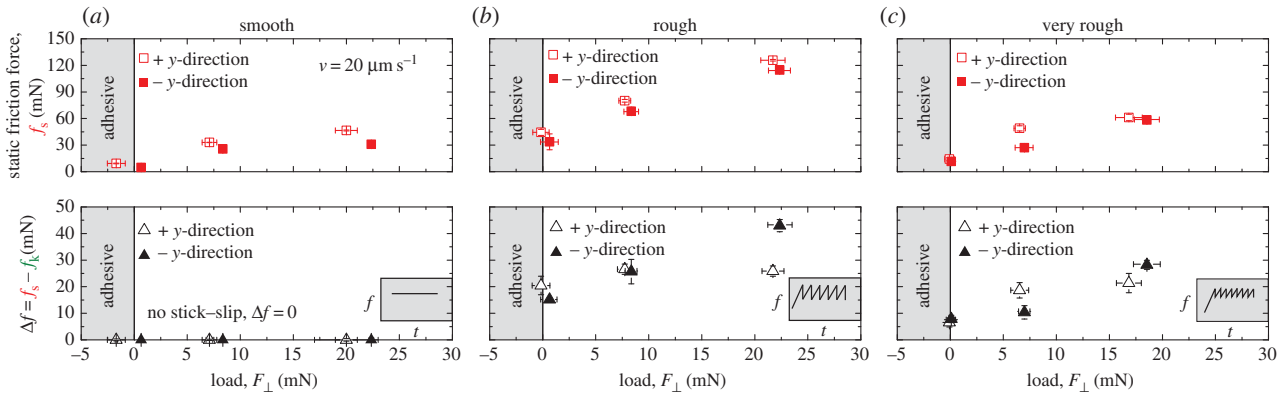

Figure 3. Plots of the static friction force (f_s 'red') as a function of the load, $F_\perp$, for three varying levels of rough surfaces (*a*,*b*,*c*) sheared at a constant velocity, $v = 20$ μm s^{-1}, in the direction along the tilt of the gecko-mimetic flaps ($+y$) and against the direction of tilt ($-y$). The lower plots depict the magnitude of stick–slip friction by the relation $\Delta f = f_s - f_k$, where f_s is the static friction force and f_k is the kinetic friction force. The error bars indicate the standard deviation in the measurements from three different experiments including the variations in a given experiment (figure 2*b*). (Online version in colour.)

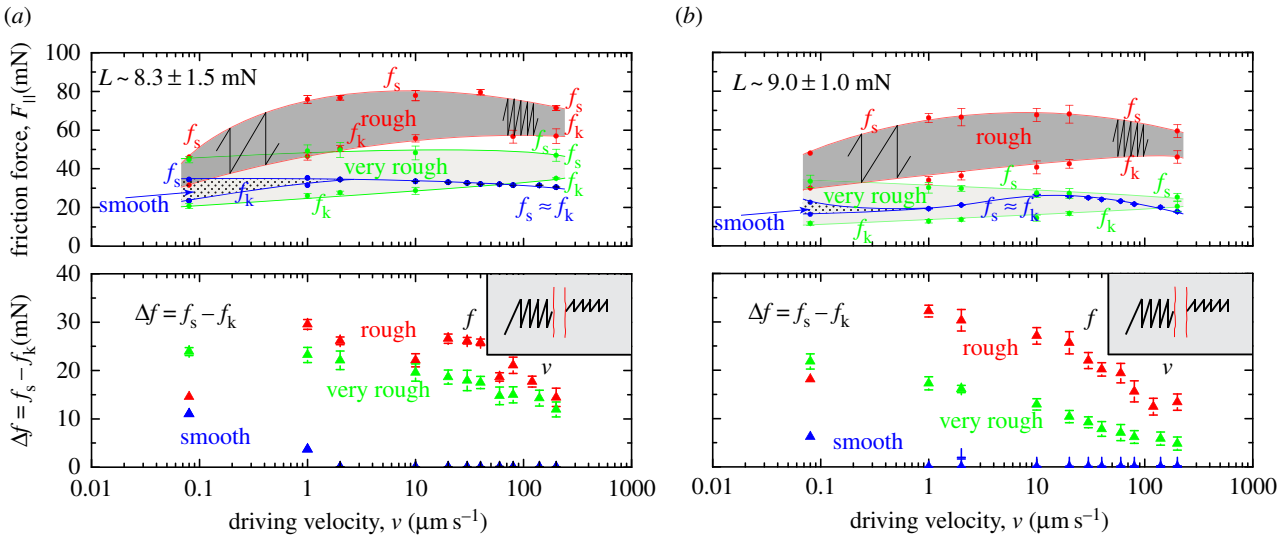

Figure 4. Plots of the static friction force (f_s) and kinetic friction force (f_k) from the friction traces as a function of the shear driving velocity, v, for three different rough surfaces of varying roughness (smooth (blue), rough (red) and very rough (green)) sheared at a constant load in the direction (*a*) along ($+y$-direction) and (*b*) against ($-y$-direction) the tilt of the tilted PDMS flaps. The lower plot depicts the magnitude of stick–slip friction by the relation $\Delta f = f_s - f_k$, where f_s is the static friction force and f_k is the kinetic friction force. (Online version in colour.)

The flaps display maximum stick–slip during sliding on the rough silica surface, which is as high as double that of the very rough disc. At higher loads, the magnitude of stick–slip is greater for shearing along the $-y$-direction (against the tilt of the flaps) compared with the $+y$-direction (along the tilt of the flaps).

2.2. Effect of shear drive velocity on friction force

The tilted PDMS microflaps do not undergo stick–slip sliding ($\Delta f = f_s - f_k = 0$) against a smooth silica disc for $F_\perp \leq 20$ mN and $v \geq 20$ μm s^{-1}; however, at lower driving velocities ($v = 0.08$–20 μm s^{-1}), the surfaces exhibit stick–slip motion ($\Delta f > 0$; figure 4). Stick–slip is always present for shearing the microflaps against the rough and the very rough silica discs. The rough disc displays an increasing and then decreasing magnitude of stick–slip with increasing velocity (red triangles in figure 4). The magnitude of Δf is similar for shearing the flaps along the $+y$- and $-y$-direction on the rough discs. The very rough disc shows a higher magnitude of Δf along the $+y$-direction relative to the $-y$-direction of shear.

Interestingly, even though the magnitude of stick–slip friction typically decreases with increasing velocities, the static friction force does not change significantly. This is contrary to a typical stick–slip phenomenon between sliding surfaces where the static force decreases to the magnitude of kinetic friction. In these experiments, the kinetic friction force is thus increasing to match the static friction force values.

2.3. Friction map

Depending on the nature of motion between the microflaps and the silica surface, a map can be constructed to indicate the regime of smooth sliding conditions and stick–slip friction (figure 5). The transition from stick–slip motion to smooth sliding is observed only when the microflaps are sheared against a smooth silica surface. The surfaces always show stick–slip friction between the flaps and the rough or the very rough surfaces in the velocity regime of the measurements. However, it should be noted that the magnitude of stick–slip decreases with increasing velocity during shearing, indicating that the sliding will eventually show a smooth

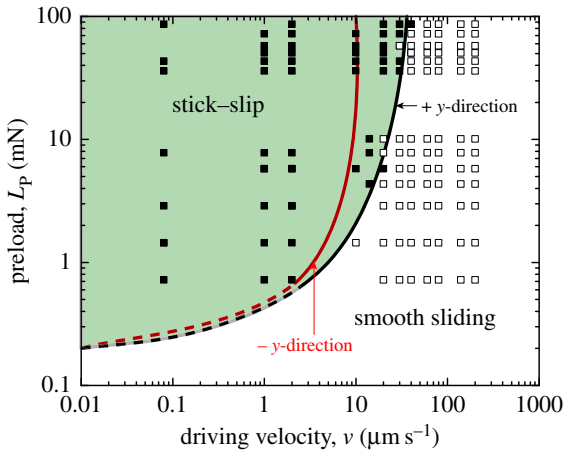

Figure 5. Friction map depicting stick–slip and smooth sliding regimes for the $+y$ (along the tilt) and $-y$ (against the tilt) shearing directions as a function of pre-load and driving velocity, v, for a smooth glass disc. Increasing driving velocity leads to smooth sliding. The dashed line is a continuation of the solid curve and extends in a regime where theoretically, for extremely low loads and low velocities, stick–slip during sliding should disappear; however, it cannot be measured due to experimental limitations. (Online version in colour.)

motion for high shearing velocities. The 'smooth sliding' regions of the friction map may be interpreted as an indicator for the operating conditions of sliding velocities when actuating the foot of a robot with the gecko-mimetic pad attached to enable a secure stick to a surface and easy release. These results also stress the importance of the sliding distance during the operation of a gecko-mimetic footpad on robotic devices and are discussed later.

3. Discussion

Two very interesting phenomena are evident from the friction force measurements as a function of load. First, the rough surfaces exhibit the highest friction forces and stick–slip magnitude. This can be explained through an interlocking mechanism [33] (figure 6) where the roughness of the surface matches with the interspacing of the array of flaps. Based on the values in table 1, the average distance between asperities on the rough surface (6.7 ± 3.5 μm) shows that it is possible to fit the flap dimensions ($10\ \mu m \times 3.5\ \mu m$) in between some spots where the asperities are more spread out. The interlocking mechanism and fitting of flaps between surface asperities are compared in figure 6. The smooth disc does not have these asperities, and the very rough disc has asperities too large and close together to allow for interlocking to occur. Another feature present in the data is that the friction values for the smooth and very rough surfaces are very comparable. It appears that the friction between the flaps and the pair of surfaces (smooth and very rough) follows Amontons' law, which states that friction forces are independent of the apparent area of contact. Molecular dynamics simulations suggest that for non-adhering surfaces above a certain load, the coefficient of friction is independent of the detailed nature of the surface roughness [34]. These surfaces have previously been tested for adhesion and exhibit adhesion only once the surfaces have been sheared [4,16]. The very rough surfaces contain asperities that are too close together and too large for the full interlocking mechanism to take place, thus allowing Amontons' law to hold true.

3.1. Stick–slip mechanism: the avalanche model

Here, we present the *avalanche model* which explains that stick–slip instabilities at the macrolevel are initiated by the micro-instabilities at the contact junction between the individual microflaps and the silica surface (figure 7*a*,*b*). Stick–slip at individual microcontacts between two 'dry' surfaces in relative motion ensues owing to creep instabilities [35,36], brittle fracture [37,38] or viscoelastic shear failure [39] of the interlocked asperities as they detach (figure 7*a*).

The creep instability mechanism assumes that the stick–slip magnitude ($\Delta f = f_s - f_k$) is determined by the size of the contact area and not by f_s or the shear force required to break the adhesive interface. Even though the *apparent* area of the contact between the smooth silica surface and the PDMS flaps is larger than that between the rough/very rough discs for the same load, stick–slip sliding disappears when shearing the PDMS flaps against the smooth silica surface, unlike sliding on the rough/very rough surface. Hence, creep instability is not a plausible explanation for the stick–slip in our system. A brittle fracture mechanism can also be ruled out, because the contact under consideration is soft and deformable. During sliding of the PDMS flaps on the silica surface, viscoelastic instability causes the contact junction to grow when the surfaces slide past each other, and the friction force (or stress) increases during this stage from f_k to f_s. Depending on the relative displacement between the sliding surfaces, the contact junction dilates and breaks when a critical stress is reached, leading to a crack-like contact instability followed by the release of the elastic strain energy at the contact junction.

The trailing edge of a contact junction is associated with detachment of the individual flaps from the silica surface in a JKR peeling fashion [4,5]. The flaps that are about to detach from the silica surface are shown in red in figure 7*b*,*d*. When a critical stress is reached for a few microflaps at the contact boundary, they detach and trigger other near critical detachments, and the surfaces slip for a distance d or nd, where d = distance between the arrays of the flaps and n is an integer (see the electronic supplementary material, figure S2). The slip is also associated with the propagation of Schallamach [40,41] waves from the front to the rear end of the contact. This propagation causes the viscoelastic PDMS flaps to release the shear stresses at the trailing edge of the contact junction and stick at the advancing edge of the contact to the silica surface. Hence, each slip is associated with a Schallamach wave and the frequency of stick–slip (φ) is equal to the rate of propagation of the waves. Each of these slips is associated with an increase and decrease in the apparent contact junction area and is evident from the sliding video footage (see the electronic supplementary video).

When Schallamach waves are responsible for the peeling (JKR mechanism) [4,5] and sticking of an adhesive interface, the work of adhesion can be estimated by

$$F_{\|} v \sim \frac{f_s + f_k}{2} v = A_{app} \Delta W \varphi, \tag{3.1}$$

where φ is frequency of the Schallamach waves (s^{-1}), ΔW is work of adhesion during *avalanche stick–slip* (or energy dissipated during *avalanche rupture* of the adhesive interface, not the thermodynamic work of adhesion) between the surfaces (J m^{-2}), v is velocity of the driving surface (m s^{-1}) and A_{app} is the apparent area of contact (m^2).

The work of adhesion for the shearing of the flaps against the silica surfaces was estimated using equation (3.1). It should be noted that the rate of shearing affects the work

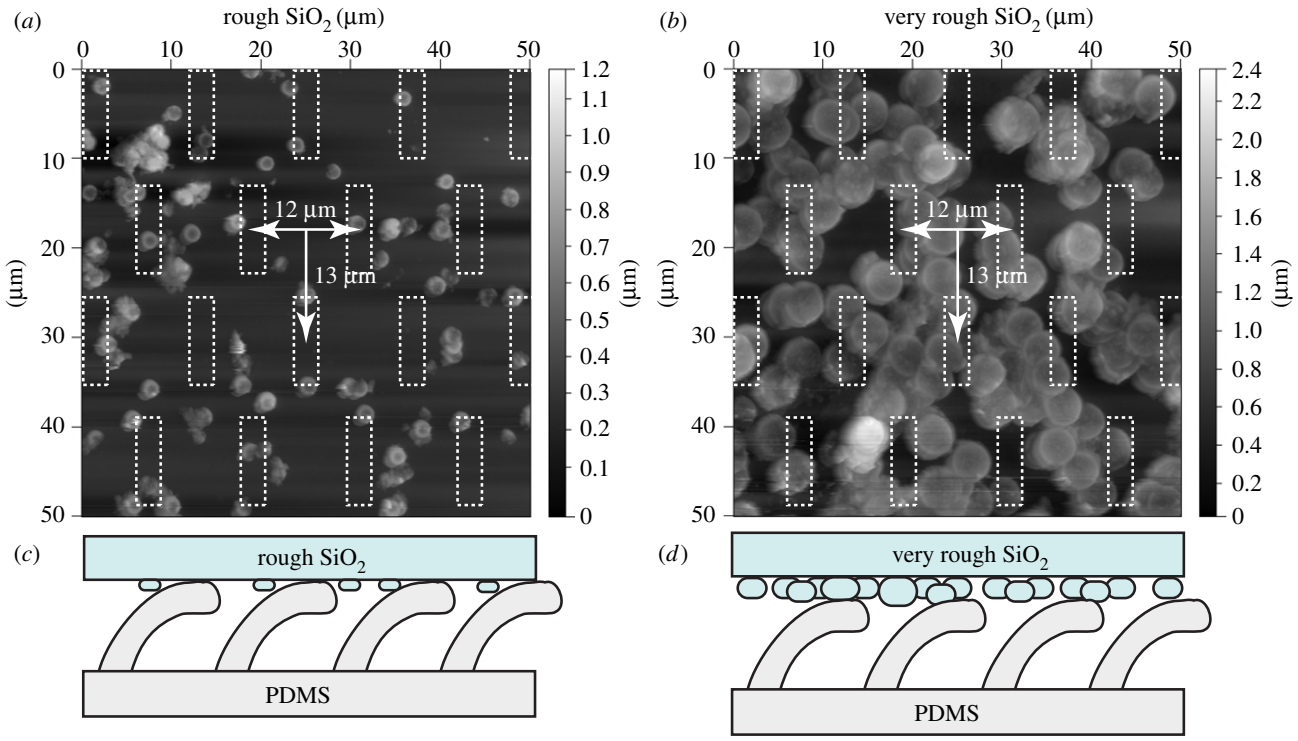

Figure 6. Atomic force microscopy images of the rough surfaces ((*a*) rough and (*b*) very rough) with an overlay of the gecko flap tip dimensions and spacing. The interlocking mechanism is displayed schematically where the rough disc (*c*) and PDMS flaps have commensurate spacing compared with the very rough disc (*d*), starting to approximate a 'smooth' surface. (Online version in colour.)

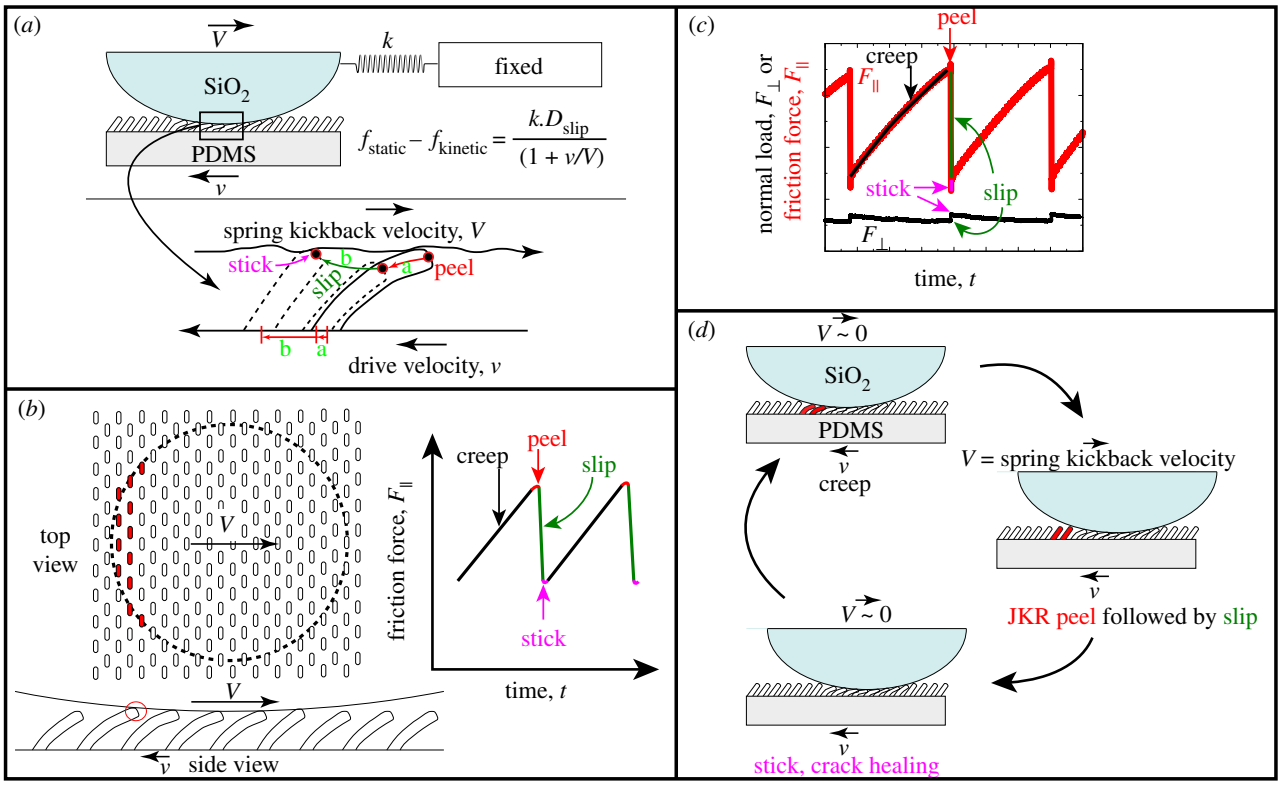

Figure 7. The *avalanche* stick–slip of the arrays of PDMS flaps from the silica surface. (*a*) The PDMS microflaps peeling (JKR) from the silica surface during the *avalanche* slip at the microscale that causes the force measuring spring to kickback with a velocity *V*. (*b*) The flaps that are about to detach from the silica surface are shown in red along with a cartoon of the stick–slip friction trace showing the creep, JKR-peel, slip and stick regimes. (*c*) An illustration of the normal load ($F_{\perp}$) and friction force ($F_{||}$) measured in the SFA during shearing of the microflaps against a silica surface showing the different regimes (creep, JKR-peel, slip and stick) during the *avalanche* slip. It should be noted that the load fluctuates during sliding along the $+y$- and $-y$-directions similar to that observed for gecko setae [8]. (*d*) *Avalanche* slip as visualized at the macroscale when the spherical silica surface is sheared against the PDMS microflaps. (Online version in colour.)

of adhesion drastically over five orders of magnitude (see the electronic supplementary material, figure S3). Energy dissipation (ΔW) during sliding of the surfaces is maximal for the rough silica surface compared with the smooth and the very rough silica for similar loads and shearing velocities. The calculated ΔW for $v < 1\ \mu m\ s^{-1}$ is less than the

thermodynamic work of adhesion between silica and PDMS, because thermal energy provides a mechanism for the interfacial bonds between the surfaces to overcome a fixed energy barrier during the slow shearing process [25,42]. We also find that the energy dissipation shows a linear relationship with the sliding velocity (v) (electronic supplementary material, figure S3).

The relative slip distance, D_{slip}, between the flaps and the silica surface can be used to characterize stick–slip friction. To calculate this value, the velocities of the two surfaces (v = drive velocity (m s^{-1}), V = spring kickback velocity in the *opposite* direction of shear (m s^{-1})) and time during the slip, t_{slip} (s), must be known, and can be related by

$$D_{slip} = t_{slip}(v + V). \tag{3.2}$$

Here, the only unknown value is the spring kickback velocity, V, i.e. the average speed at which the lateral force measuring spring retracts back during the slip between the surfaces, which can be calculated from experimental data given by

$$V = \frac{f_s - f_k}{kt_{slip}}, \tag{3.3}$$

where t_{slip} is slip time (s), k is spring constant of the lateral force measuring spring (N m^{-1}), and f_s and f_k are the static and kinetic friction (N) as described previously. This is a complex relationship that also depends on surface roughness, load and shearing velocity, which affects the values of f_s and f_k as seen from figures 3 and 4.

The slip time (t_{slip}) in our experiments was 60–80 µs for $v \leq$ 10 µm s^{-1} and 40 µs for $v \geq 20$ µm s^{-1} when shearing against silica surfaces of different roughness. Thus, the *avalanche* slip is characterized by a specific slip distance ($D_{slip} = nd$) and slip times (t_{slip}). The slip distance, D_{slip}, is more dependent on the flap spacing compared with the distribution of silica surface asperities, because D_{slip} shows similar length scales when sliding against both the rough and very rough surfaces (electronic supplementary material, figure S2). The slip times are dependent on the elastic material properties of the flap's surface, where they are equivalent regardless of the surface roughness. These characteristic length and time scales give rise to a stick–slip sliding behaviour that is less reliant on the commensurability between the shearing surfaces; however, the surface commensurability is a crucial property that determines the magnitude of friction (and adhesion) forces [33].

While shearing the PDMS microflaps against the silica surfaces (both smooth and rough), $f_s - f_k$ decreased and f_k increased as v was increased (figure 4). When sliding against the smooth surface, $f_s - f_k \to 0$ for $v > 20$ µm s^{-1} (figures 4 and 5). However, we did not observe smooth sliding for the rough and the very rough silica surfaces for $v = 0.08$–200 µm s^{-1} at all loads, L, tested. Theoretically, higher sliding velocities are required to reach the smooth sliding regime ($\Delta f = f_s - f_k = 0$), which were not attainable owing to the limitations of the apparatus. A guaranteed approach to eliminate stick–slip in this system would be to only shear the surfaces for a specified distance, $D < D_c$, that never reaches the highest static friction value, f_s ($D = D_c$ at f_s), where stick–slip initiates. Clearly, from the experiments performed, f_s varies as a function of load and velocity, which indicates that the critical distance, D_c, would also change based on the varying loads and velocities. Hence, an all-encompassing D_c should be the smallest sliding distance for any load and velocity combination tested prior to a stick–slip event. This will ensure that the surface does not shear past an f_s limit. The distance D_c can easily be calculated from the experiment as the average time it takes for f_k to transition to f_s multiplied by the shearing drive velocity, v. In our experiments, we calculate this critical sliding distance to be $D_c \leq 40$ µm for the rough surface and less than or equal to 15 µm for the very rough surface to encompass all $v = 0.08$–200 µm s^{-1} and $L = 1$–20 mN. Thus, to avoid *slip* failure on a rough surface, a robot with the reversible gecko-mimetic adhesive footpads should be sheared for a distance less than the critical sliding distance. To avoid slip failure on a smooth surface, it is simpler to increase the sliding velocity $v > 20$ µm s^{-1} for all loads examined in this study.

4. Conclusion

In this work, we demonstrate the effect of roughness and shearing velocities ($v = 0.08$–200 µm s^{-1}) on the stick–slip friction between tilted PDMS microflaps and silica surfaces. We show that Amontons' law is obeyed when the shearing between both smooth and very rough silica surfaces against the tilted microflaps. The flaps showed similar values for the static friction for shearing against the smooth and the very rough silica surfaces, and were characterized with an *avalanche* stick–slip friction model with energy dissipation showing a linear relationship with the sliding velocity. Stick–slip sliding was always observed ($\Delta f = f_s - f_k > 0$) when shearing the flaps on the rough and very rough surfaces. Sliding the microflaps on the rough surface showed maximum Δf owing to the interlocking–detachment cycles of the flaps with the surface asperities. The characteristic avalanche slip distances and times are determined by the topography and elastic properties respectively of the patterned flaps, and are independent of the commensurability between the surfaces. However, the commensurability determines the magnitude of friction.

Stick–slip friction is detrimental to the performance of the gecko-mimetic adhesives, because slipping would result in the failure of the contact, and not allow the surfaces to grip again in the absence of a restoring force. Stick–slip friction of flaps on smooth surfaces can be eliminated by increasing the sliding velocity above a critical value ($v_c = 20$ µm s^{-1} in our experiments). The friction between the microflaps and the smooth silica surface was translated into a 'friction' map that may be interpreted as an indicator for the conditions of desirable sliding velocities when actuating the foot of a robot with the gecko-mimetic pad to enable both a secure stick to a surface and easy release. Stick–slip between the rough surfaces and the flaps can be eliminated by shearing the surfaces for a distance less than D_c, which is 40 µm and 15 µm for the rough and the very rough surfaces, respectively. However, quantitative micromechanical mechanisms that can predict the critical distances (D_c) and sliding velocities (v_c) to circumvent stick–slip friction need further investigation and theoretical modelling based on the interface stiffness and topographical commensurability of the interacting surfaces. Our results stress the importance of the pre-loads, shearing distance, commensurability, sliding direction and velocities for the safe operation of gecko-mimetic footpads on robotic devices.

5. Experimental

Large arrays of tilted PDMS microflaps with an areal density of 6410 flaps mm^{-2} mimicking the adhesive and frictional

properties of a gecko footpad were fabricated and have been described elsewhere [16,33]. A modified SFA (SurForce LLC) [16,43] was used to measure the normal $F_{\perp}$ (adhesion and loads) and the lateral forces $F_{||}$ between the arrays of the fabricated microflaps and a spherical silica disc of radius of curvature $R = 2$ cm, and three different RMS roughnesses of 10 ± 8 nm (smooth), 133 ± 20 nm (rough) and 308 ± 56 nm (very rough). The detailed characterization of the roughnesses is given in table 1. Details of the force measurements have been described in previous work [16,33]. Briefly, the spherical glass disc was mounted to the top friction device that measures the lateral forces $F_{||}$ on the fabricated flaps. The PDMS flaps were glued to a flat glass disc, which sits on a double cantilever spring with strain gauges that can measure the normal forces. The double cantilever spring was mounted on a bimorph device that can slide laterally over a distance of 1–700 μm at different sliding speeds (0.01–200 μm s^{-1}). A CCD camera was mounted on a microscope to visualize the contact area during loading, unloading and sliding of the spherical silica disc against the arrays of the fabricated PDMS microflaps.

In the SFA experiment, the PDMS microflaps were pressed against the top spherical silica disc at a constant speed of approximately 10 μm s^{-1} until the desired pre-load L was reached. The flaps were then sheared against the smooth and the rough spherical glass disc at different velocities (0.08–200 μm s^{-1}). Stick–slip friction force and the instantaneous normal loads $F_{\perp}$ were measured simultaneously. The measured normal load $F_{\perp}$ was different from the applied pre-load L during sliding owing to the deformation of the microflaps and adhesion/interlocking of the flaps to the glass surface. The flaps did not get damaged even after many sliding cycles (100–1000) at a given contact point and the friction force was reproducible between different contact points on the flap surface. The surfaces were prepared in a clean, dust-free environment (under laminar flow hood).

Acknowledgements. The fabrication of the microflaps and rough surfaces was supported by the Institute for Collaborative Biotechnologies through grant W911NF-09-0001 from the US Army Research Office (fabricated by S.D. and S.C.). The content of the information does not necessarily reflect the position or the policy of the Government, and no official endorsement should be inferred. The development of the three-dimensional SFA and measurements of frictional adhesion were supported by the US Department of Energy, Office of Basic Energy Sciences, Division of Materials Sciences and Engineering under award no. DE-FG02-87ER-45331 (J.N.I. for instrument modification, S.D. and N.C. for the friction measurements). The fabrication of the PDMS flaps was done in the UCSB nanofabrication facility, part of the NSF-funded National Nanotechnology Infrastructure Network (NNIN). The scanning electron microscopy and atomic force microscopy images (the latter by Y.K.) were taken at the MRL Shared Experimental Facilities which is supported by the MRSEC Programme of the National Science Foundation under award NSF DMR 1121053; a member of the NSF-funded Materials Research Facilities Network.

References

1. Autumn K, Liang YA, Hsieh ST, Zesch W, Chan WP, Kenny TW, Fearing R, Full RJ. 2000 Adhesive force of a single gecko foot-hair. *Nature* **405**, 681–685. (doi:10.1038/35015073)
2. Autumn K, Peattie AM. 2002 Mechanisms of adhesion in geckos. *Integr. Comp. Biol.* **42**, 1081–1090. (doi:10.1093/icb/42.6.1081)
3. Autumn K *et al*. 2002 Evidence for van der Waals adhesion in gecko setae. *Proc. Natl Acad. Sci. USA* **99**, 12 252–12 256. (doi:10.1073/pnas.192252799)
4. Das S, Chary S, Yu J, Tamelier J, Turner KL, Israelachvili JN. 2013 JKR theory for the stick slip peeling and adhesion hysteresis of gecko mimetic patterned surfaces with a smooth glass surface. *Langmuir* **29**, 15 006–15 012. (doi:10.1021/La403420f)
5. Gillies AG, Fearing RS. 2014 Simulation of synthetic gecko arrays shearing on rough surfaces. *J. R. Soc. Interface* **11**, 20140021. (doi:10.1098/rsif.2014.0021)
6. Autumn K, Dittmore A, Santos D, Spenko M, Cutkosky M. 2006 Frictional adhesion: a new angle on gecko attachment. *J. Exp. Biol.* **209**, 3569–3579. (doi:10.1242/Jeb.02486)
7. Puthoff JB, Holbrook M, Wilkinson MJ, Jin K, Pesika NS, Autumn K. 2013 Dynamic friction in natural and synthetic gecko setal arrays. *Soft Matter* **9**, 4855–4863. (doi:10.1039/C3sm50267h)
8. Zhao BX, Pesika N, Rosenberg K, Tian Y, Zeng HB, McGuiggan P, Autumn K, Israelachvili J. 2008 Adhesion and friction force coupling of gecko setal arrays: implications for structured adhesive surfaces. *Langmuir* **24**, 1517–1524. (doi:10.1021/la702126k)
9. del Campo A, Greiner C, Arzt E. 2007 Contact shape controls adhesion of bioinspired fibrillar surfaces. *Langmuir* **23**, 10 235–10 243. (doi:10.1021/la7010502)
10. Gao H, Wang X, Yao H, Gorb S, Arzt E. 2005 Mechanics of hierarchical adhesion structures of geckos. *Mech. Mater.* **37**, 275–285. (doi:10.1016/j.mechmat.2004.03.008)
11. Peng Z, Chen S. 2012 The effect of geometry on the adhesive behavior of bio-inspired fibrils. *Soft Matter* **8**, 9864–9869. (doi:10.1039/c2sm26390d)
12. Gravish N *et al*. 2010 Rate-dependent frictional adhesion in natural and synthetic gecko setae. *J. R. Soc. Interface* **7**, 259–269. (doi:10.1098/rsif.2009.0133)
13. Canas N, Kamperman M, Volker B, Kroner E, McMeeking RM, Arzt E. 2012 Effect of nano- and micro-roughness on adhesion of bioinspired micropatterned surfaces. *Acta Biomater.* **8**, 282–288. (doi:10.1016/j.actbio.2011.08.028)
14. Geim AK, Dubonos SV, Grigorieva IV, Novoselov KS, Zhukov AA, Shapoval SY. 2003 Microfabricated adhesive mimicking gecko foot-hair. *Nat. Mater.* **2**, 461–463. (doi:10.1038/Nmat917)
15. Murphy MP, Kim S, Sitti M. 2009 Enhanced adhesion by gecko-inspired hierarchical fibrillar adhesives. *ACS Appl. Mater. Interfaces* **1**, 849–855. (doi:10.1021/Am8002439)
16. Yu J, Chary S, Das S, Tamelier J, Pesika NS, Turner KL, Israelachvili JN. 2011 Gecko-inspired dry adhesive for robotic applications. *Adv. Funct. Mater.* **21**, 3010–3018. (doi:10.1002/adfm.201100493)
17. Zhou M, Pesika N, Zeng HB, Wan J, Zhang XJ, Meng YG, Wen SZ, Tian Y. 2012 Design of gecko-inspired fibrillar surfaces with strong attachment and easy-removal properties: a numerical analysis of peel-zone. *J. R. Soc. Interface* **9**, 2424–2436. (doi:10.1098/rsif.2012.0200)
18. Xue L, Kovalev A, Thöle F, Rengarajan GT, Steinhart M, Gorb SN. 2012 Tailoring normal adhesion of arrays of thermoplastic, spring-like polymer nanorods by shaping nanorod tips. *Langmuir* **28**, 10 781–10 788. (doi:10.1021/la3020354)
19. Heepe L, Gorb S. 2014 Biologically inspired mushroom-shaped adhesive microstructures. *Annu. Rev. Mater. Res.* **44**, 173–203. (doi:10.1146/annurev-matsci-062910-100458)
20. Kim Y, Claus RK, Limanto F, Fearing RS, Maboudian R. 2013 Friction characteristics of polymeric nanofiber arrays against substrates with tailored geometry. *Langmuir* **29**, 8395–8401. (doi:10.1021/la400641a)
21. Rodriguez I, Lim CT, Natarajan S, Ho AYY, Van EL, Elmouelhi N, Low HY, Vyakarnam M, Cooper K. 2013 Shear adhesion strength of gecko-inspired tapes on surfaces with variable roughness. *J. Adhesion* **89**, 921–936. (doi:10.1080/00218464.2013.767198)
22. Asbeck A, Dastoor S, Parness A, Fullerton L, Esparza N, Soto D, Heyneman B, Cutkosky M. 2009 Climbing rough vertical surfaces with hierarchical directional adhesion. In *IEEE Int. Conf. on Robotics and Automation, Kobe, Japan, 12–17 May 2009,* pp. 2675–2680. (doi:10.1109/ROBOT.2009.5152864)
23. Chen S, Gao H. 2007 Bio-inspired mechanics of reversible adhesion: orientation-dependent adhesion

strength for non-slipping adhesive contact with transversely isotropic elastic materials. *J. Mech. Phys. Solids* **55**, 1001–1015. (doi:10.1016/j.jmps.2006.10.008)

24. Yao H, Della Rocca G, Guduru PR, Gao H. 2008 Adhesion and sliding response of a biologically inspired fibrillar surface: experimental observations. *J. R. Soc. Interface* **5**, 723–733. (doi:10.1098/rsif.2007.1225)
25. Israelachvili JN. 2011 *Intermolecular and surface forces,* revised 3rd edn. San Diego, CA: Academic Press.
26. Rabinowicz E. 1965 *Friction and wear of materials*. New York, NY: Wiley.
27. Tambe NS, Bhushan B. 2005 Friction model for the velocity dependence of nanoscale friction. *Nanotechnology* **16**, 2309–2324. (doi:10.1088/0957-4484/16/10/054)
28. Yoshizawa H, Israelachvili J. 1993 Fundamental mechanisms of interfacial friction 0.2. Stick–slip friction of spherical and chain molecules. *J. Phys. Chem.* **97**, 11 300–11 313. (doi:10.1021/J100145a031)
29. Israelachvili J, Berman A. 1995 Irreversibility, energy dissipation, and time effects in intermolecular and surface interactions. *Isr. J. Chem.* **35**, 85–91. (doi:10.1002/ijch.199500014)
30. Berman AD, Ducker WA, Israelachvili JN. 1996 Origin and characterization of different stick–slip friction mechanisms. *Langmuir* **12**, 4559–4563. (doi:10.1021/la950896z)
31. Yoshizawa H, Mcguiggan P, Israelachvili J. 1993 Identification of a second dynamic state during stick–slip motion. *Science* **259**, 1305–1308. (doi:10.1126/science.259.5099.1305)
32. Tysoe W, Spencer N. 2004 Why does Amontons' law work so well? *Tribol. Lubr. Technol.* **60**, 64.
33. Yu J, Chary S, Das S, Tamelier J, Turner KL, Israelachvili JN. 2012 Friction and adhesion of gecko-inspired PDMS flaps on rough surfaces. *Langmuir* **28**, 11 527–11 534. (doi:10.1021/La301783q)
34. Gnecco E, Meyer E. 2007 *Fundamentals of friction and wear*. Berlin, Germany: Springer.
35. Ishlinskii AY, Kragel'skii IV. 1944 Rapid changes during friction. *Zh. Tekh. Fiz.* **14**, 276–282.
36. Scholz CH, Engelder JT. 1976 Role of asperity indentation and plowing in rock friction 0.1. Asperity creep and stick–slip. *Int. J. Rock Mech. Min.* **13**, 149–154. (doi:10.1016/0148-9062(76)90819-6)
37. Byerlee JD. 1967 Theory of friction based on brittle fracture. *J. Appl. Phys.* **38**, 2928–2934. (doi:10.1063/1.1710026)
38. Carlos Miguez Suarez J, Biasotto Mano E. 2000 Brittle–ductile transition of gamma-irradiated recycled polyethylenes blend. *Polym. Test.* **19**, 607–616. (doi:10.1016/S0142-9418(99)00031-8)
39. Scholz CH. 2002 *The mechanics of earthquakes and faulting*. Cambridge, UK: Cambridge University Press.
40. Schallamach A. 1963 A theory of dynamic rubber friction. *Wear* **6**, 375–382. (doi:10.1016/0043-1648(63)90206-0)
41. Schallam A. 1971 How does rubber slide? *Wear* **17**, 301–312. (doi:10.1016/0043-1648(71)90033-0)
42. Golden J. 1975 A molecular theory of adhesive rubber friction. *J. Phys. A, Math. Gen.* **8**, 966–979. (doi:10.1088/0305-4470/8/6/015)
43. Israelachvili J *et al*. 2010 Recent advances in the surface forces apparatus (SFA) technique. *Rep. Prog. Phys.* **73**, 036601. (doi:10.1088/0034-4885/73/3/036601)